SCIENTIFIC REPORTS

Three-dimensional Monte Carlo model of the coffee-ring effect in evaporating colloidal droplets

A. Crivoi & Fei Duan

School of Mechanical and Aerospace Engineering, Nanyang Technological University, Singapore 639798.

The residual deposits usually left near the contact line after pinned sessile colloidal droplet evaporation are commonly known as a "coffee-ring" effect. However, there were scarce attempts to simulate the effect, and the realistic fully three-dimensional (3D) model is lacking since the complex drying process seems to limit the further investigation. Here we develop a stochastic method to model the particle deposition in evaporating a pinned sessile colloidal droplet. The 3D Monte Carlo model is developed in the spherical-cap-shaped droplet. In the algorithm, the analytical equations of fluid flow are used to calculate the probability distributions for the biased random walk, associated with the drift-diffusion equations. We obtain the 3D coffee-ring structures as the final results of the simulation and analyze the dependence of the ring profile on the particle volumetric concentration and sticking probability.

The coffee-ring effect has been observed in various experiments with different colloidal suspensions[1–16], including polymers[2–4], quantum dots[5], nanoparticles[6–10], bacteria[11], and biofluids[12–16], such as urine[14], blood[15], and serum[16]. The effect has initially been investigated by Deegan et al.[17] and explained as a ubiquitous phenomenon caused by the replenishing outward capillary flow and uneven evaporation rate[18,19]. The previous attempts to simulate the effect were commonly based on the numerical techniques, such as the finite-element method[20], applying the analytical equations to figure out the evolution of the average particle density profile. Another family of approaches, based on the Monte Carlo methods, uses randomly distributed particles on the discrete lattice and calculates the probabilities of the possible particle motion directions on each simulation step. One recent attempt to build a Monte Carlo model of the droplet evaporation, capillary flow and contact line deposition has been performed by Kim et al.[21]. The model used a simple power-law assumption about the particle motion on the basis of the flow analysis of Deegan et al.[17] and reproduced the contact line deposition profile[2]. However, the simulation has been limited to the simplified radial particle motion and has not considered the vertical velocity component and dependence on the vertical coordinate. In the work of Yunker et al.[22], the coffee-ring growth was modeled in two dimensions (2D) as the Poisson-like process of random particle deposition coupled with the surface diffusion. The model, focusing only on the vicinity of the contact line, has not considered the droplet evaporation and inward flow dynamics. The Monte Carlo approach based on the biased random walk (BRW) has been recently used to investigate the transition from the coffee-ring deposition towards the uniform coverage in 2D[8,9,23]. In the present work we further develop the BRW method into the more realistic 3D domain and use the flow analysis of Hu and Larsson[24–26] to calculate the corresponding probabilities of the sampled particle moves on each Monte Carlo Step (MCS). This advancement allows achieving a full 3D structure of the coffee ring and analyzing the thickness profile of the structure. The evolution of the ring shape and dimensions is observed during the entire time period of the droplet drying.

The mathematical model is based on the BRW approach[27–29] in a 3D domain with a cubical lattice structure, which mimics the shape of a pinned sessile droplet (see Fig. 1) with a spherical cap with a pre-defined initial contact angle value, θ_0, and apex height, h_0. The domain boundary surface continuously shrinks in the vertical direction during evaporation. The geometrical shape is assumed to remain spherical cap, and the contact angle value continuously decreases with time. It is assumed for simplicity that the droplet apex height reduces linearly with dimensionless time, $\tilde{t}$[26], $h(0,\tilde{t}) = h_0(1-\tilde{t})$. At the initial state, the particles are uniformly distributed inside the domain according to the defined volumetric concentration, ϕ. Afterwards, on each MCS of the simulation, each particle may perform a biased random move into a vacant cell within the domain. Each particle move is sampled from the seven-component finite set, where six elements correspond to the six possible directions of motion, and the seventh possible move is "waiting", or keeping particle position in the lattice until the next MCS.
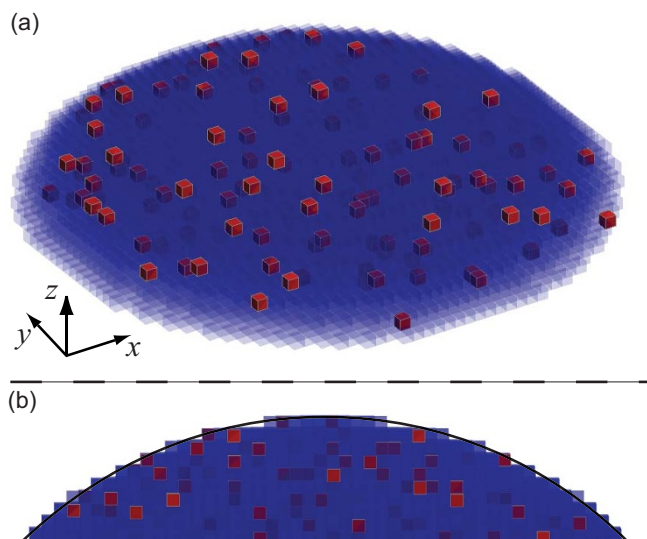
Figure 1 | The schematic representation of the 3D model implementation. The spherical cap-like volume of the cubical lattice is filled with liquid (blue) and randomly distributed particles (red cubes). (a) shows the isometric view of the modeled droplet, and (b) shows the side view of the droplet.

To calculate the probabilities corresponding to the chance of drawing a given direction for a particle, first of all, the dimensionless velocity components $\tilde{v}_x$, $\tilde{v}_y$, $\tilde{v}_z$ are calculated from the analytical expressions[25,26] for each particle (see the details in the Methods section). The velocity values significantly depend on time and the particle position, rising near the three-phase domain boundary. Meanwhile, the lattice configuration restricts the simulated particle displacement with one lattice cell at one MCS. Therefore, the duration of each MCS might be different, and the tick size of the clock for $\tilde{t}$ is adjusted to the fastest moving particle. The drift velocities of the slower particles are scaled by the factor of velocity of the fastest particle. Thus all the rescaled velocities fall in the range between 0 and 1, and the preliminary probability distribution of the sampled move directions can be calculated. However, one more important modification implementing the "waiting" moves is required to keep the diffusion parameter consistent in a BRW model with a strong bias[28,29]. It has to be remembered that the random Brownian (or un-biased) displacement is dependent on the duration of MCS. Therefore, shorter simulation steps corresponding to the faster drift velocities should have lower probabilities of moving in any direction, different from the direction of $\tilde{v}$. Lowering the diffusion component without changing the drift component results in increasing the wait-ing probability during the current MCS[27]. Finally, seven probability components are re-calculated for each particle on each MCS, $p_{move} = \{p_{x_+}, p_{x_-}, p_{y_+}, p_{y_-}, p_{z_+}, p_{z_-}, p_w\}$; the subscripts x, y, z indicate the three Cartesian axes, "+" and "−" signs indicate whether this direction matches the direction of $\tilde{v}$ projection on this axis or is opposite, and p_w is the probability of the "waiting" move. Once p_{move} is determined, the direction of the current move is sampled from the biased distribution.

An additional method is used to improve the convergence of the simulation run. Since the velocity value near the three-phase line region becomes very high, especially at later stages, the direct scaling by the maximum velocity may lead to the MCS duration approaching zero, and hence reaching the end of the evaporation process at $\tilde{t} = 1$ may require an infinite number of MCS. To avoid this divergence, the particles reaching the three-phase contact line or inner side of the coffee ring are excluded from calculations of the maximum velocity. It is reasonable, since the outwardly moving particles reaching the

domain boundary are not able to move further, and their actual velocity becomes zero. The same situation happens with the particles reaching the boundary coffee-ring composed from the blocked part-icles at the later stages. Even if the analytical equations show a high $\tilde{v}$ value for such a particle, the model rules do not allow it to move into the occupied cells, and the particle may be excluded from the simu-lated dynamics. Therefore, the duration of current MCS is calculated based on the velocities of all the other particles which have not yet been blocked by the boundaries.

The model is also considering the possible particle agglomeration into clusters on each MCS. An additional parameter, p_{stick}, controls the sticking probability of the particles. The mechanics of the process is implemented according to the Diffusion Limited Aggregation (DLA) rules[8,9,23]. The aggregated particles continue their further motion as one inseparable object (cluster), and their averaged posi-tion is used to calculate p_{move} and sample the corresponding dir-ection. The aggregation event is the binary random variable sampled for the particles occupying the neighbouring cells with the probability equal to $p_{stick} \cdot (\Delta \tilde{t})$, where p_{stick} is fixed during the run, and $\Delta \tilde{t}$ is the duration of current MCS. Particles reasonably have higher aggregation chance during the longer time steps.

Results

The simulations are performed using the following values of the fixed parameters: the droplet base diameter is set to 500 cells; the initial contact angle value, θ_0, is assumed to be $\pi/4$; the non-dimensional particle size is $1 \times 1 \times 1$ cells; and the dimensionless initial evap-orative flux at the droplet apex is fixed at $\tilde{J}(0,0) = 1$. The volumetric particle concentration, ϕ, and sticking parameter, p_{stick}, are varied in consecutive simulation runs to investigate the influence on the cof-fee-ring shape and final particle distribution. Figure 2 presents the results of a sample simulation run with ϕ at 0.01. The image sequence shows the progression of the droplet evaporation and the coffee-ring forming process. The process starts with the uniform particle distri-bution inside the spherical cap (see Fig. 2 (a)), then the droplet consequently shrinks while the ring starts to build up (Figs. 2 (b–h)); at the later stages the rest of the particles joins the ring structure and completes the inner ring side (Fig. 2 (i–r)), finally only very few particles are left inside the ring, and the droplet completely dries out (Fig. 2 (s–t)). The final image of the ring well resembles some pre-vious experimental observations[8].

The investigation of the coffee-ring shape dependence on the par-ticle concentration and sticking probability is performed as well. Figure 3 displays the final results of the multiple simulations with the different particle concentrations varying from 0.01 to 0.05, and p_{stick} values at 0.1 (a–b rows in Fig. 3) and 1.0 (c–d rows). Image collection (Fig. 3 (a1–a5)) presents a gradual increase of the ring width with the rising number of particles in case of low sticking p_{stick} = 0.1. Figure 3 (b1–b5) shows that only small clusters, indicated by different color, are formed in these cases, and most of the particles do not stick together. The shape of the ring looks generally smooth, and the width rapidly grows with increasing ϕ. However, increasing the sticking chances ten-fold to $p_{stick} = 1$ provides visible changes in the final ring structure for higher particle concentrations (Fig. 3 (c3–c5)). More particles stick together to form slower moving clusters, thus slightly distorting the inner ring boundary and increasing the particle presence near the domain center. Cluster diagrams in Fig. 3 (d1–d5) show that $p_{stick} = 1$ is high enough to cause forming of a large ring aggregate for $\phi > 0.01$. Differently, the coffee rings in insets Fig. 3 (a1–a5) for $p_{stick} = 0.1$ are composed from multiple small clusters or separate particles (Fig. 3 (b1–b5)). The diagrams in Fig. 4 present thickness profiles of the final results corresponding to Fig. 3. The comparison between color maps shows that thickness of ring struc-tures is distributed rather similarly for $p_{stick} = 0.1$ (shown in Fig. 4 (a1–a5)) and $p_{stick} = 1$ (shown in Fig. 4 (b1–b5)). However, the thickness of the rings with a low sticking changes very gradually,
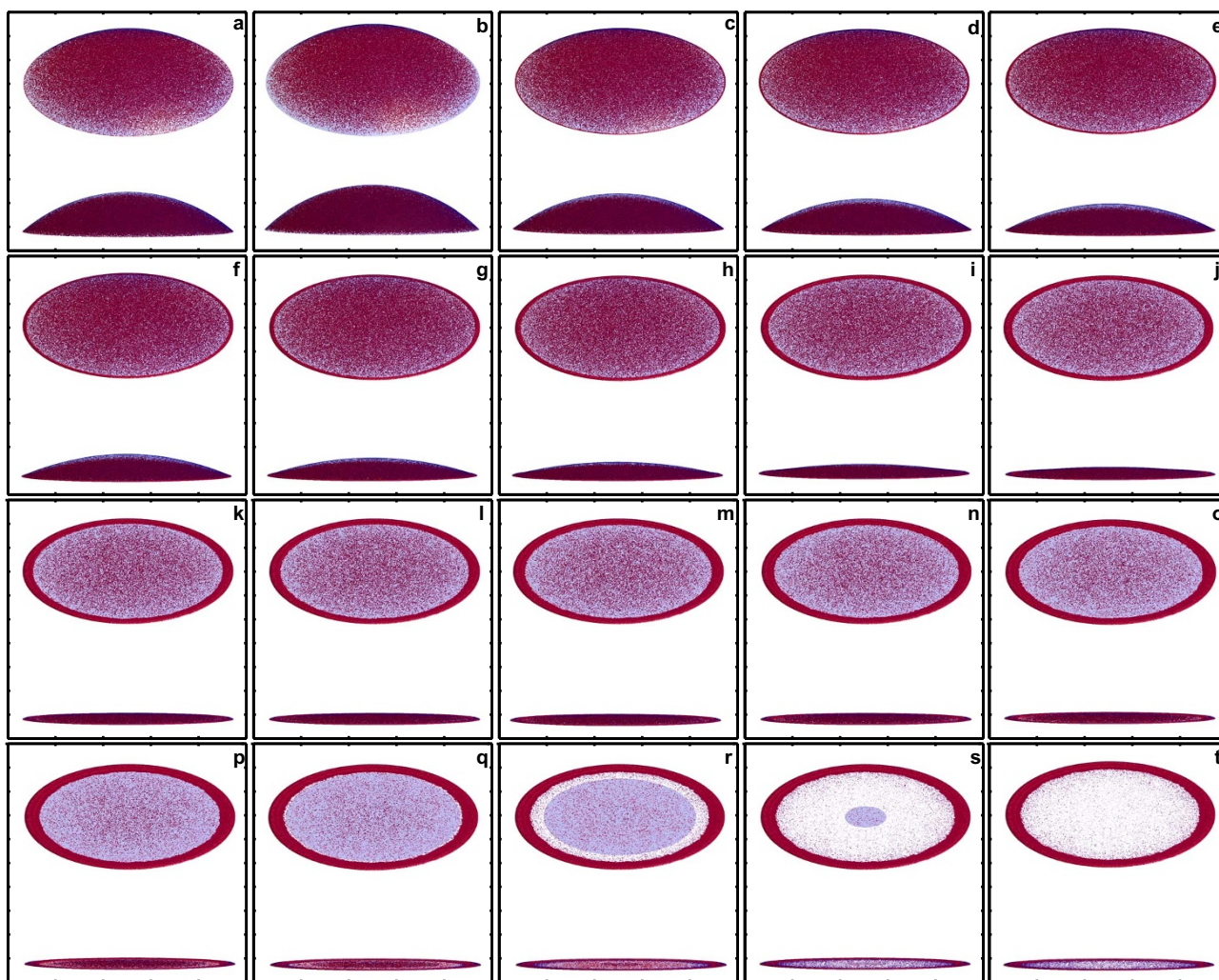
Figure 2 | The progression of the single droplet drying process over time in a Monte Carlo simulation run. (a) shows the initial system state at $\tilde{t} = 0.001$ from isometric view (top image) and side view (bottom image); (b–t) show the corresponding images of the drying droplet after (b) $\tilde{t} = 0.1$, (c) $\tilde{t} = 0.2$, (d) $\tilde{t} = 0.3$, (e) $\tilde{t} = 0.4$, (f) $\tilde{t} = 0.5$, (g) $\tilde{t} = 0.6$, (h) $\tilde{t} = 0.7$, (i) $\tilde{t} = 0.8$, (j) $\tilde{t} = 0.85$, (k) $\tilde{t} = 0.9$, (l) $\tilde{t} = 0.91$, (m) $\tilde{t} = 0.92$, (n) $\tilde{t} = 0.93$, (o) $\tilde{t} = 0.94$, (p) $\tilde{t} = 0.96$, (q) $\tilde{t} = 0.97$, (r) $\tilde{t} = 0.98$, (s) $\tilde{t} = 0.99$, (t) $\tilde{t} = 1$. The full animations are available as the Supplementary Video-1 for the isometric view and Supplementary Video-2 for the side view.

reaching the peak closer to the three-phase line and decreasing towards the domain center (Fig. 4 (a4–a5)). Meanwhile, higher sticking leads to the emergence of more complex branched aggregates for $\phi > 0.03$ (Fig. 4 (b4–b5)), thus slightly distorting the profile of the ring. The corresponding curves in Fig. 4 (a6–b6) indicate a higher particle presence inside the ring for high-sticking and high-concentration results (Fig. 4 (b4–b5)).

Discussion

The presented algorithm might serve as a simplistic basis for developing more specific or sophisticated models, potentially including the effects of Marangoni convection, solution viscosity, etc. There are several additional important rules considering the particle mechanics in the presented model, worth mentioning: 1. The particles are not allowed to overlap with each other (conservation of the global particle concentration, ϕ). This rule allows particles to stack onto each other and form a solid structure. 2. Once the particle leaves the droplet domain as a result of the droplet shrinking, the only allowed move is in the vertical down direction, unless the underlying cell is occupied by the other particle or substrate. This restriction prevents the particle diffusion in the absence of liquid but allows the

particles drop due to the gravity. 3. All the moves outside the current domain are prohibited (the barrier boundary condition). Thus, the simulation starts at $\tilde{t} = 0$ with the particles randomly distributed inside the volume of the spherical cap with $\tilde{h} = 1$ and finishes at $\tilde{t} = 1$, $\tilde{h} = 0$ with the particles immobilized on the empty substrate or atop the other particles.

To summarize, the coffee-ring effect is simulated in the 3D domain, while including both particle diffusion and the capillary particle transport towards the three-phase contact line. The spatial domain of the model is the evaporating sessile droplet represented as a spherical cap. The time scale of the simulation is the full drying process, from the placement of the drop onto a substrate till the final dry-out of the remaining solvent. The simulation result provides a full 3D model of the coffee ring, and the vertical ring thickness profile is measured. The final shape of the simulated ring structure shows a reasonable dependence on the volumetric particle concentration and colloidal aggregation parameter.

Methods

The distribution $p_{move} = \{p_{x_+}, p_{x_-}, p_{y_+}, p_{y_-}, p_{z_+}, p_{z_-}, p_w\}$ for each particle is deduced from the dimensionless velocity components as
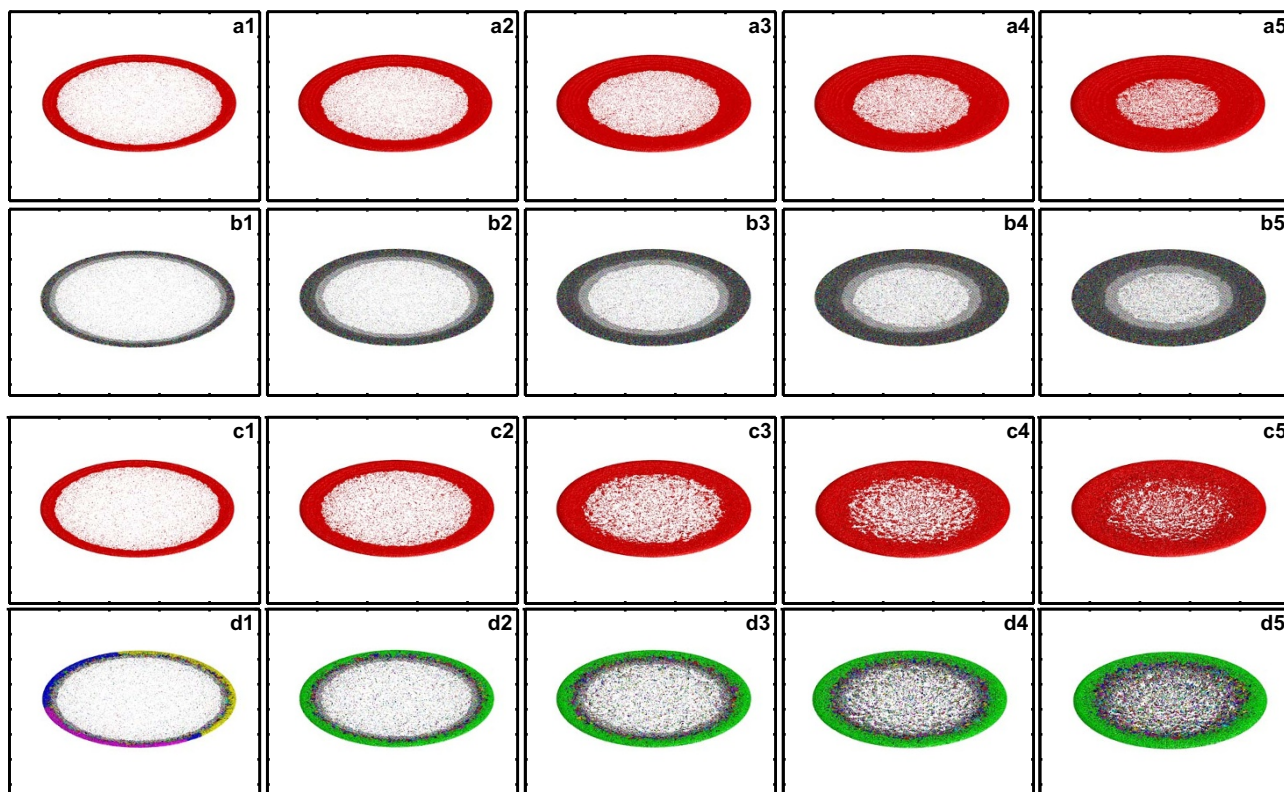
Figure 3 | Aggregated simulation results showing the final coffee-ring structures for different volumetric particle concentrations and sticking parameter values. (a1–a5) show the final dried states corresponding to particle concentrations, ϕ, at (a1) 0.01, (a2) 0.02, (a3) 0.03, (a4) 0.04, (a5) 0.05, and sticking parameter value $p_{stick} = 0.1$. The remaining particles are shown in red color. (b1–b5) show the cluster diagrams corresponding to the results from (a1–a5). Different particle clusters are indicated by different colors. The small size of the clusters is caused by a very low particle sticking probability. (c1–c5) show the final dried states corresponding to particle concentrations, ϕ, at (c1) 0.01, (c2) 0.02, (c3) 0.03, (c4) 0.04, (c5) 0.05, and sticking parameter value $p_{stick} = 1$, particles are shown in red. (d1–d5) show the cluster diagrams corresponding to the results from (c1–c5). The main, ring-shaped aggregate is seen in (d2–d5) and indicated with green color. Other, smaller clusters are seen inside the main ring and are more evident for the highest particle concentration in (d5).

$$\left\{ \begin{array}{l} p_{x_-} = \frac{1}{2N\tilde{v}_{max}} - \frac{\tilde{v}_x}{2N\tilde{v}_{max}^2} \\[4pt] p_{x_+} = \frac{1}{2N\tilde{v}_{max}} - \frac{\tilde{v}_x}{2N\tilde{v}_{max}^2} + \frac{\tilde{v}_x}{N\tilde{v}_{max}} \\[4pt] p_{y_-} = \frac{1}{2N\tilde{v}_{max}} - \frac{\tilde{v}_y}{2N\tilde{v}_{max}^2} \\[4pt] p_{y_+} = \frac{1}{2N\tilde{v}_{max}} - \frac{\tilde{v}_y}{2N\tilde{v}_{max}^2} + \frac{\tilde{v}_y}{N\tilde{v}_{max}} \\[4pt] p_{z_-} = \frac{1}{2N\tilde{v}_{max}} - \frac{\tilde{v}_z}{2N\tilde{v}_{max}^2} \\[4pt] p_{z_+} = \frac{1}{2N\tilde{v}_{max}} - \frac{\tilde{v}_z}{2N\tilde{v}_{max}^2} + \frac{\tilde{v}_z}{N\tilde{v}_{max}} \\[4pt] p_w = 1 - p_{x_-} - p_{x_+} - p_{y_-} - p_{y_+} - p_{z_-} - p_{z_+} \end{array} \right\}, \qquad (1)$$

where $N = 3$ for 3D space, $\tilde{v}_{max} > 1$ is the dimensionless velocity of the fastest particle, $\tilde{v}_x$, $\tilde{v}_y$ and $\tilde{v}_z$ are the dimensionless velocity components, calculated from the analytical equations for the liquid flow[25,26]:

$$\left\{ \begin{array}{l} \tilde{v}_r(\tilde{r},\tilde{z},\tilde{t}) = \frac{3}{8}\frac{1}{1-\tilde{t}}\left[(1-\tilde{r}^2) - (1-\tilde{r}^2)^{-\lambda(\theta)}\right]\left(\frac{\tilde{z}^2}{\tilde{h}^2} - 2\frac{\tilde{z}}{\tilde{h}}\right) - \frac{gh_0\tilde{h}}{2R}\left(\frac{\tilde{z}}{\tilde{h}} - \frac{3}{2}\frac{\tilde{z}^2}{\tilde{h}^2}\right), \\[6pt] \tilde{v}_z(\tilde{r},\tilde{z},\tilde{t}) = \frac{3}{4}\frac{1}{1-\tilde{t}}\left[1 + \lambda(\theta)(1-\tilde{r}^2)^{-\lambda(\theta)-1}\right]\left(\frac{\tilde{z}^2}{3h^2} - \frac{\tilde{z}^3}{h}\right) + \frac{3}{2}\frac{1}{1-\tilde{t}}\left[(1-\tilde{r}^2) - (1-\tilde{r}^2)^{-\lambda(\theta)}\right] \\[6pt] \qquad \left(\frac{\tilde{z}^2}{2h^2} - \frac{\tilde{z}^3}{3h^3}\right)\tilde{h}(0,\tilde{t}) + \frac{gh_0}{4\tilde{r}}\left(\tilde{z}^2 - \frac{\tilde{z}^3}{h}\right) + \frac{g'h_0}{4}\left(\tilde{z}^2 - \frac{\tilde{z}^3}{h}\right) - \frac{g'h_0\tilde{r}}{2}\frac{\tilde{z}^3}{h^2}\tilde{h}(0,\tilde{t}), \\[6pt] g(\tilde{r},\tilde{t}) = -2h_0\tilde{r}\left(\tilde{J}(\tilde{t})\lambda(\theta)(1-\tilde{r}^2)^{-\lambda(\theta)-1} + 1\right) - f(Ma,\Delta T,v), \end{array} \right\} \quad (2)$$

where the dimensionless variables are defined: radial velocity $\tilde{v}_r = v_r t_f/R$, vertical velocity $\tilde{v}_z = v_z t_f/R$, time $\tilde{t} = t/t_f$, radial coordinate $\tilde{r} = r/R$, vertical coordinate $\tilde{z} = z/h_0$, and liquid layer thickness $\tilde{h} = h/h_0$, in which t_f is the total drying time, and R is the droplet base radius, $\lambda(\theta)$ is linearly dependent on the current contact angle value θ, $\lambda(\theta) = 1/2 - \theta/\pi$; g' is the first-order partial derivative of the function, $g(\tilde{r},\tilde{t})$, with $\tilde{r}$; $\tilde{J} = \tilde{J}(0,\tilde{t})$ is the dimensionless evaporative flux at the top of the droplet surface, $\tilde{J} \propto \left(0.27\theta^2 + 1.3\right)\left(0.6381 - 0.2239\left(\theta - \frac{\pi}{4}\right)^2\right)$ according to Hu and Larsson[26], and $f(Ma, \Delta T, v)$ is a Marangoni effect function of the cumulative influence of the

temperature and surfactant gradients. Our simulations show that low dimensionless values of f ($f < 5$) do not significantly affect the final structures, therefore f term is neglected in the presented results ($f = 0$). The influence of the strong Marangoni effect ($f > 5$) on the coffee-ring structures in 3D is a subject for future study. The expressions of $\tilde{v}_r$ and $\tilde{v}_z$ are calculated for each particle and recalculated for each MCS, then the horizontal velocity components in x and y directions are simply derived from projections $v_x = v_r x/r$ and $v_y = v_r y/r$.

The maximal absolute value of the particle velocity $\tilde{v}_{max}$ on a given MCS is taken as maximum $max(\tilde{v}_x, \tilde{v}_y, \tilde{v}_z)$ from all the calculated particle velocity components. Particles reaching the domain boundary or the coffee ring are excluded from this calculation, since their actual velocity vanishes.

Cluster-cluster aggregation is performed by examining each individual cluster for neighbouring particles from the other clusters. If the particles are present in the neighbouring cells, the binary variable is sampled with probability of $p_{stick}\cdot(\Delta\tilde{t})$, $\Delta\tilde{t}$ is calculated from $\Delta\tilde{t} = 1/(NB\tilde{v}_{max})$, in which B is the number of cells in the lattice radius (250 in the current work). If the sampled variable is 1, the aggregation occurs, and on the next MCS the aggregated particles move together as a whole cluster.

The tick size of the simulation clock at a given MCS, $\Delta\tilde{t}$, is adjusted to the fastest particle with $\tilde{v}_{max}$ and also scaled by the lattice size and number of dimensions. Since the particles start to move faster towards the end of simulation, the clock slows down, and it takes more MCS for the latest drying stages. Reasonably, larger lattices also require more MCS to finish the whole simulation. The diffusion coefficient, according to Codling et al.[27], in BRW model is proportional to sum of individual move probabilities,

$$p_{x_-} + p_{x_+} + p_{y_-} + p_{y_+} + p_{z_-} + p_{z_+} = 1 - p_w = \frac{N\tilde{v}_{max} - (\tilde{v}_x + \tilde{v}_y + \tilde{v}_z) + (\tilde{v}_x + \tilde{v}_y + \tilde{v}_z)\tilde{v}_{max}}{N\tilde{v}_{max}^2} \quad (3)$$

Therefore, shorter MCS with a larger $\tilde{v}_{max}$ have smaller random displacement caused by the Brownian motion. The waiting probability, p_w, can be alternatively expressed as,

$$p_w = \frac{(N\tilde{v}_{max} - (\tilde{v}_x + \tilde{v}_y + \tilde{v}_z))(\tilde{v}_{max} - 1)}{N\tilde{v}_{max}^2} \quad (4)$$
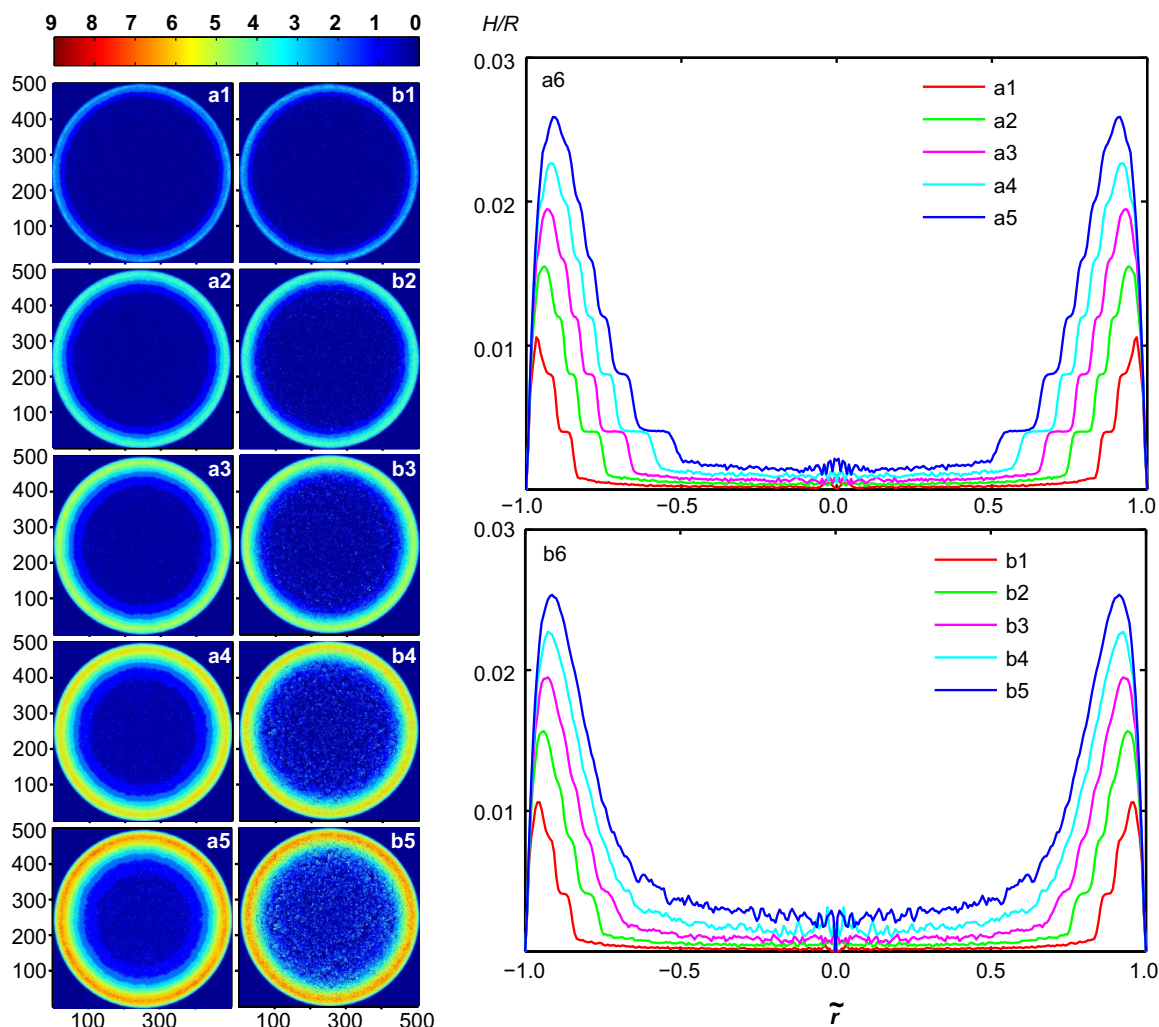
Figure 4 | Analysis of the height profiles of the structures presented in Fig. 3. (a1–a5) show the color maps of the particle structure height corresponding to particle concentrations, ϕ, from (a1) 0.01 to (a5) 0.05, and $p_{stick} = 0.1$. (b1–b5) show the corresponding maps for different sticking $p_{stick} = 1$. The color bar shows the dependence of the height value on the displayed color. Minimal height shown is 0 (empty area), maximum height is 9, meaning that nine particle layers are stacked on each other in these cells of the lattice. The plot diagrams (a6) and (b6) show the corresponding ring thickness profiles depending on the distance from the domain center. The ring height is averaged over the all cross-sectional directions. H is the height of the particle layer, $\tilde{r}$ is the non-dimensional distance from the base center, and R is the base radius respectively.

It shows that for the fastest possible particle with $(\tilde{v}_{max}, \tilde{v}_{max}, \tilde{v}_{max})$ some move definitely happens ($p_w = 0$); and if all the particles are slow ($\tilde{v}_{max} = 1$), there is no waiting on the current MCS. In the actual simulations $\tilde{v}_{max}$ is almost always higher than 1. However, if this condition is not fulfilled, the probabilities are not rescaled by $\tilde{v}_{max}$. Then the condition ($p_w = 0$) is used, and the equations for the slow drift $\tilde{v}/\tilde{v}_{max}$ of the form $p = \frac{1}{2N} \pm \frac{\tilde{v}_{(x,y,z)}}{2N\tilde{v}_{max}}$ are used to calculate p_{move}, in which $\tilde{v}_{(x,y,z)}$ is the projection value on x, y, or z axis respectively.

1. Dou, R. & Derby, B. Formation of coffee stains on porous surfaces. *Langmuir* **28**, 5331 (2012).
2. Conway, J., Korns, H. & Fisch, M. R. Evaporation kinematics of polystyrene bead suspensions. *Langmuir* **13**, 426–431 (1997).
3. Soltman, D. & Subramanian, V. Inkjet-printed line morphologies and temperature control of the coffee ring effect. *Langmuir* **24**, 2224–2231 (2008).
4. Yunker, P. J., Still, T., Lohr, M. A. & Yodh, A. G. Suppression of the coffee-ring effect by shape-dependent capillary interactions. *Nature* **476**, 308–311 (2011).
5. Maenosono, S., Dushkin, C. D., Saita, S. & Yamaguchi, Y. Growth of a semiconductor nanoparticle ring during the drying of a suspension droplet. *Langmuir* **15**, 957–965 (1999).
6. Bigioni, T. P. *et al.* Kinetically driven self assembly of highly ordered nanoparticle monolayers. *Nat. Mater.* **5**, 265–270 (2006).
7. Choi, S., Stassi, S., Pisano, A. P. & Zohdi, T. I. Coffee-ring effect-based three dimensional patterning of micro/nanoparticle assembly with a single droplet. *Langmuir* **26**, 11690–11698 (2010).
8. Crivoi, A. & Duan, F. Amplifying and attenuating the coffee-ring effect in drying sessile nanofluid droplets. *Phys. Rev. E* **87**, 042303 (2013).
9. Crivoi, A. & Duan, F. Effect of surfactant on the drying patterns of graphite nanofluid droplets. *J. Phys. Chem. B* **117**, 5932–5938 (2013).
10. Crivoi, A. & Duan, F. Fingering structures inside the coffee-ring pattern. *Colloid Surf. A - Physicochem. Eng. Asp.* **432**, 119126 (2013).
11. Sempels, W., Dier, R. D., Mizuno, H., Hofkens, J. & Vermant, J. Auto-production of biosurfactants reverses the coffee ring effect in a bacterial system. *Nat. Commun.* **4**, 1757 (2013).
12. Yakhno, T. Salt-induced protein phase transitions in drying drops. *J. Colloid Interface Sci.* **318**, 225–230 (2008).
13. Shabalin, V. N. & Shatokhina, S. N. Diagnostic markers in the structures of human biological liquids. *Singapore Med. J.* **48**, 440–446 (2007).
14. Yakhno, T. A., Yakhno, V. G., Sanin, A. G., Sanina, O. A. & Pelyushenko, A. S. Protein and salt: spatiotemporal dynamics of events in a drying drop. *Tech Phys+* **49**, 1055–1063 (2004).
15. Brutin, D., Sobac, B., Loquet, B. & Sampol, J. Pattern formation in drying drops of blood. *J. Fluid Mech.* **667**, 8595 (2011).
16. Zhuang, H., Coulepis, A. G., Locarnini, S. A. & Gust, I. D. Detection of markers of hepatitis b infection in serum dried on to filter-paper: an application to field studies. *Bull. World Health Organ.* **60**, 783–787 (1982).
17. Deegan, R. D. *et al.* Capillary flow as the cause of ring stains from dried liquids. *Nature* **389**, 827–829 (1997).
18. Deegan, R. D. Pattern formation in drying drops. *Phys. Rev. E* **61**, 475–485 (2000).
19. Deegan, R. D. *et al.* Contact line deposits in an evaporating drop. *Phys. Rev. E* **62**, 756–765 (2000).

20. Bhardwaj, R., Fang, X. & Attinger, D. Pattern formation during the evaporation of a colloidal nanoliter drop: a numerical and experimental study. *New J. Phys.* **11**, 075020 (2009).

21. Kim, H.-S., Park, S. S. & Hagelberg, F. Computational approach to drying a nanoparticle-suspended liquid droplet. *J. Nanopart. Res.* **13**, 59–68 (2010).

22. Yunker, P. J. *et al.* Effects of particle shape on growth dynamics at edges of evaporating drops of colloidal suspensions. *Phys. Rev. Lett.* **110**, 035501 (2013).

23. Crivoi, A. & Duan, F. Elimination of the coffee-ring effect by promoting particle adsorption and long-range interaction. *Langmuir* **29**, 1206712074 (2013).

24. Hu, H. & Larson, R. G. Marangoni effect reverses coffee-ring depositions. *J. Phys. Chem. B* **110**, 7090–7094 (2006).

25. Hu, H. & Larson, R. G. Analysis of the effects of marangoni stresses on the microflow in an evaporating sessile droplet. *Langmuir* **21**, 3972–3980 (2005).

26. Hu, H. & Larson, R. G. Analysis of the microfluid flow in an evaporating sessile droplet. *Langmuir* **21**, 3963–3971 (2005).

27. Codling, E. A., Plank, M. J. & Benhamou, S. Random walk models in biology. *J. R. Soc. Interface* **5**, 813–834 (2008).

28. Gauthier, M. G. & Slater, G. W. A new set of Monte Carlo moves for lattice random-walk models of biased diffusion. *Physica A* **355**, 283–296 (2005).

29. Gauthier, M. G. & Slater, G. W. Building reliable lattice Monte Carlo models for real drift and diffusion problems. *Phys. Rev. E* **70**, 015103 (2004).

Acknowledgments

Author contributions

A.C. and F.D. prepared the manuscript and the figures. Both authors reviewed the manuscript.

Additional information

Supplementary information accompanies this paper at http://www.nature.com/scientificreports

Competing financial interests: The authors declare no competing financial interests.

How to cite this article: Crivoi, A. & Duan, F. Three-dimensional Monte Carlo model of the coffee-ring effect in evaporating colloidal droplets. *Sci. Rep.* **4**, 4310; DOI:10.1038/srep04310 (2014).